NUMERICAL OPTIMIZATION OF AN EJECTOR FOR WASTE HEAT RECOVERY USED TO COOL DOWN THE INTAKE AIR IN AN IC ENGINE

José Galindo, Antonio Gil, Vicente Dolz, Alberto Ponce-Mora

CMT – Motores Térmicos, Universitat Politècnica de València, Spain

Abstract

In the present paper, a numerical investigation of a jet-ejector is carried out using a real gas model of R1234yf. The prototype under investigation works with specific operating conditions of a jet-ejector refrigeration system intended for waste heat recovery in an internal combustion engine. In the first instance, the geometry optimization involving nozzle exit diameter, mixing chamber diameter and nozzle exit position is performed. Once the optimum geometry has been obtained, the jet-ejector prototype is tested with different operating pressure ratios to determine its off-design performance. The flow structure in relevant cases has been examined with an emphasis on critical and subcritical modes. The flow phenomena occurring during expansion, entrainment and mixing processes are discussed so performance degradation can be directly related to physical processes. The analysis has been completed fitting simulated points to critical and subcritical planar surfaces. The results in terms of goodness of fit are satisfactory so the jet-ejector performance in off-design operating conditions can be reflected through simple mathematic models. When the overall cycle is assessed by using previous CFD maps it is observed that the achievable cooling drops significantly when an ambient temperature of 31 $°C$ is exceeded.

Keywords

Waste heat recovery, jet-ejector cycle, adiabatic engine, jet-ejector optimization, engine efficiency, R1234yf

Nomenclature

Acronyms

ICE	Internal Combustion Engine
CFD	Computational Fluid Dynamics
COP	Coefficient Of Performance
GWP	Global Warming Potential

Notation

Latin

A	Area (m^2)
c	Specific Heat Capacity (J/kg·K)
D	Diameter (mm)
h	Specific enthalpy (J/kg)
k	Pump pressure ratio (-)
L	Length (mm)
$\dot{m}$	Mass flow rate (kg/s)
P	Pressure (bar)
$\dot{Q}$	Heat exchanger power (W)
$\dot{W}$	Mechanical power (W)
Z	Mesh zone

30 **Greek letters**

α	Angle (°)
β	Curve fit coefficient (-)
κ	Fraction of the available heat power at the exhaust line (-)
λ	Jet-ejector scaling factor (-)
π	Jet-ejector pressure ratio (-)
ω	Entrainment ratio (-)

31 **Subscripts**

$1-8$	Cycle state points
$\mathrm{I}-\mathrm{VI}$	Generic index
amb	Ambient conditions
$crit$	Jet-ejector critical operational mode
e	Jet-Ejector
ev	Ejection cycle evaporator
ex	Engine exhaust
ft	Curve fitting
ge	Ejection cycle generator
i	Inlet flow
in	Engine intake
max	Maximum
o	Outlet flow
OD	Off-design conditions
p	Primary flow

pm	Ejection cycle pump
ref	Reference conditions
s	Secondary flow
$scrit$	Ejector subcritical operational mode
sm	Simulated
sup	Superheating temperature
v	Expansion valve

1. INTRODUCTION

Over the past decades, many research projects have focused on the improvement of ejection cycles in search of a refrigeration technology with lower environmental impact. Ejection cycles seem to be a promising way of taking advantage of low-grade waste heat coming from industrial processes, vehicle exhaust or solar energy reducing significantly the electric power consumed by conventional refrigeration systems.

In comparison with traditional vapor-compression refrigeration systems, they present lower mechanical complexity as well as improved reliability and lifespan (Varga et al., 2009; Yan et al., 2012). However, poor performance when operating in off-design conditions has been reported. This well-known factor together with their low COP is responsible for the limited market penetration up to now (He et al., 2009).

On ejection cycles, a secondary flow characterized by low temperature and pressure generates a cooling capacity at the evaporator, absorbing heat from the medium to be cooled. The primary flow, which has received energy at the generator from a low-grade heat source, expands within a nozzle at the jet-ejector inlet thereby enabling the suction of secondary flow inside the jet-ejector. Both flows mix completely, leave the jet-ejector and condense at an intermediate

50 pressure. As a result of the condensation, heat is rejected to ambient. Downstream the
51 condenser the liquid splits: a fraction of total mass flow passes through a liquid pump and the
52 resulting high-pressure fluid is recirculated to the generator thus completing the power loop.
53 The rest of the available mass flow expands at an expansion valve and evaporates closing the
54 refrigeration loop and producing the desired cooling capacity.

55 Jet-ejector improvement is a key factor to maximize the performance of ejection cycles. The
56 geometric configuration and the operating conditions dramatically affect the entrainment
57 process so a deep understanding of flow evolution inside the jet-ejector is essential. Specific
58 design for a certain application and operating conditions is needed. Both experimental,
59 numerical and analytical studies comprise the main development methodologies. Studies
60 concerning the jet-ejector design (Dong et al., 2016; Jia and Wenjian, 2012; Ruangtrakoon et al.,
61 2013; Wang et al., 2017; Yan et al., 2012; Zhu et al., 2009) and modeling (Soroureddin et al.,
62 2013) are quite common in the literature. Many research papers have been focused on studying
63 fundamental phenomena occurring inside the jet-ejector since it is the basis for improving the
64 entrainment process (Ruangtrakoon et al., 2013; Sargolzaei et al., 2010; Zhu and Jiang, 2014a,
65 2014b).

66 When applied to a vehicle this energy-efficient cycle is developed within the framework of
67 different strategies of waste heat recovery (WHR) dedicated to reusing the exhaust waste heat.
68 In the last few years, the need for cleaner vehicles with lower environmental impact is leading
69 to a growing interest in these technologies. On an internal combustion engine (ICE) for
70 automotive applications, approximately one-third of available fuel energy is lost as exhaust
71 waste heat and an additional one third is rejected to ambient at the cooling water system.
72 Several approaches have been under investigation to unlock this potential (Armstead and Miers,
73 2013) with special emphasis on: Intake charge heating, applied specifically during warm-up
74 process (Luján et al., 2016), turbocompounding systems (Aghaali and Ångström, 2015),

thermoelectric generators (Hsiao et al., 2010; In and Lee, 2016), Rankine cycles (Aly, 1988; Dolz et al., 2012; J. Galindo et al., 2015; Glover et al., 2014), ejection or absorption cycles (Galindo et al., 2019; Novella et al., 2017; Zegenhagen and Ziegler, 2015a) and Brayton, Stirling or Ericsson cycles (J Galindo et al., 2015).

The feasibility of cooling down the engine intake by using a jet-ejector cycle with R134a as working fluid has been studied before by Zegenhagen and Ziegler (Zegenhagen and Ziegler, 2015a), (Zegenhagen and Ziegler, 2015b) following an experimental approach. The attained cooling capacities ranged between 2.3 kW and 5.3 kW with charge air temperatures ranging between 270.8 K and 284.8 K depending on boundary conditions. Recently, Galindo et al. (Galindo et al., 2019) have evaluated and optimized numerically the performance of a jet-ejector refrigeration cycle intended for charge air cooling in an ICE. Special emphasis is put on performance degradation away from design conditions, that is, different engine operating points. They showed that ICE charge air temperature can be reduced from $\sim 40°C$ to $\sim 0°C$ if the jet-ejector size is given as a design variable. Otherwise, the achievable cooling capacity is seriously reduced.

Beyond these experimental and analytical approaches, none numerical studies have been found for this particular application. Numerous numerical studies focused on jet-ejector modeling can be found in the literature with a general approach, however, almost all of them focus on ideal gas models, (Bartosiewicz et al., 2005; Chen et al., 2013; Mazzelli et al., 2015; Ruangtrakoon et al., 2013; Sriveerakul et al., 2007) or algebraic equations of state (Mazzelli and Milazzo, 2015) since the convergence for real gas models is more complex. Some of these studies have set low operating pressures so the differences between real gas models and the aforementioned approaches might not be significant. Croquer et al. (Croquer et al., 2016), carried out simulations with real gas models (R134a) and their operating pressures are similar to those of the present paper, however, their research work is not dealing with a jet-ejector optimization and off-design

performance evaluation.

The main innovative aspect of the present paper is the geometric design and characterization of a jet-ejector implemented in a jet-ejector refrigeration system intended for intake air cooling in an ICE. As a novelty, R1234yf is used as working fluid and the performance of the optimized jet-ejector design is assessed from the perspective of the overall refrigeration system operating in off-design ambient conditions.

The main objective of this study is the numerical optimization of a jet-ejector working under specific conditions of an ICE in terms of exhaust energy and required cooling capacities. This application (ICE intake cooling) gives the work its main originality. All calculations have been performed using real gas models of a new generation refrigerant (R1234yf). As a result, a non-dimensional expression which collects information related to the geometry and off-design operating conditions is presented. The secondary objective of the present paper is to evaluate the performance degradation of the overall ejection cycle when the ambient temperature increases. For that purpose, the jet-ejector maps computed with CFD play a major role.

This methodology could be applied to introduce the jet-ejector behavior in theoretical models of the overall cycle including heat exchangers, expansion valve and pump.

2. EJECTION CYCLE INTEGRATION AND EVALUATION PROCESS

In Figure 1 a jet-ejector refrigeration system equipped in an automotive ICE is schematically illustrated. The jet-ejector refrigeration system is coupled in the ICE downstream of the intercooler and at the exhaust line downstream of the turbine. The heat exchanger placed at the engine intake is intended to produce the cooling effect at the engine intake while the generator transfers heat from the exhaust line to the refrigerant to drive the primary flow. The jet-ejector is the key element of the cycle and its limitations when adapting to off-design

operating conditions dramatically affect cycle performance. Therefore, this component plays a major role in a jet-ejector refrigeration system coupled in an ICE and its dimensions must be carefully designed for a particular cooling capacity requirement, ambient temperature and exhaust thermal level.

The logic flow chart of the steps followed in the jet-ejector characterization stage and overall cycle evaluation are schematically illustrated in Figure 2. The paper is structured in four parts. In Section 3, the jet-ejector geometry is described and the numerical setup is presented with special emphasis on boundary conditions, thermodynamic model and validation of the CFD approach. Also in Section 3, the jet-ejector dimensions involved in parametric optimization are presented. In Section 4, the theoretical model used to describe the overall system performance is presented.

In Section 5, the main results are presented. Firstly, the geometry that maximizes the entrainment ratio is found. Special attention is paid to the flow pattern in optimized and non-optimized geometries. Then, the optimum jet-ejector design is evaluated against different evaporating and condensing pressures to find the jet-ejector characteristic maps. Subsequently, the aforementioned maps are used to feed a 1D model overall cycle to assess the performance degradation that occurs when the ambient temperature is increased with a fixed jet-ejector size. Finally, in Section 6, the most relevant findings are summarized.

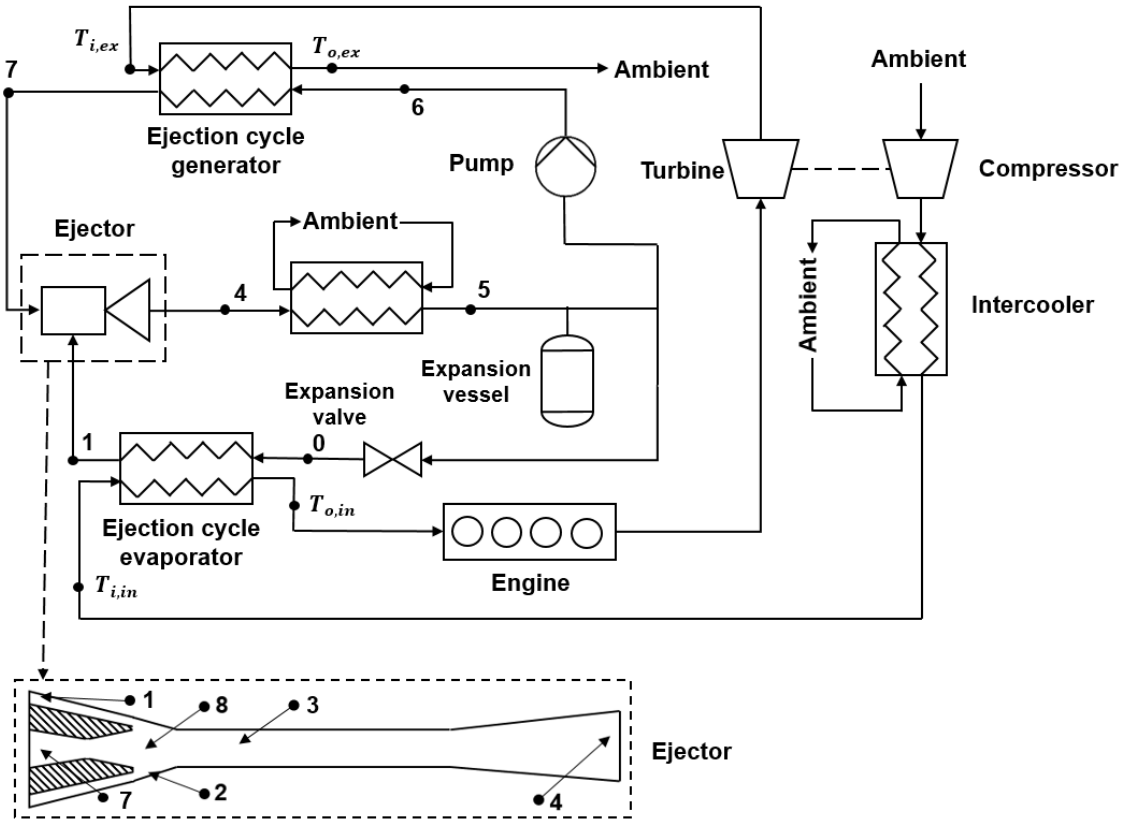

143

144 *Figure 1. Jet-ejector refrigeration system coupled in an ICE*

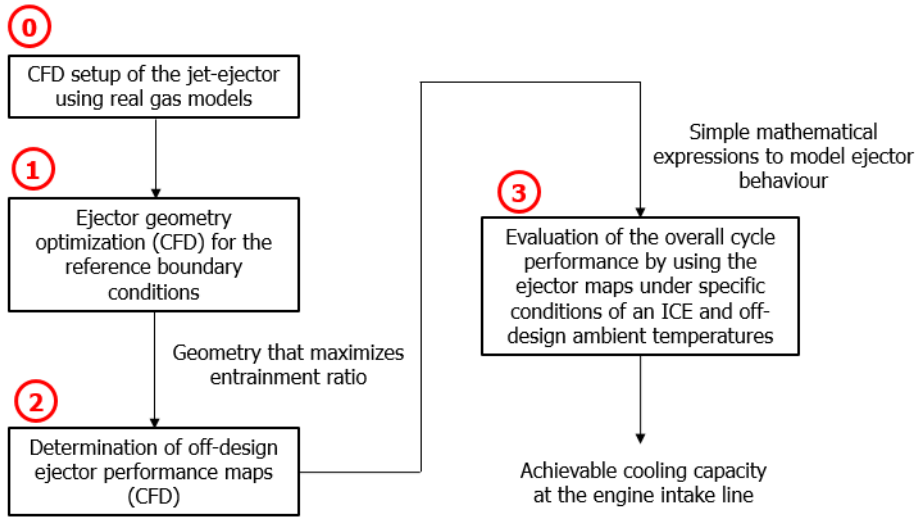

145

146 *Figure 2. Calculation sequence of the jet-ejector and the overall cycle, respectively*

147

148 # 3. JET-EJECTOR MODELING

149

In this section, the geometry of the jet-ejector prototype is presented as well as the setup in the Computational Fluid Dynamics (CFD) code including the descriptions of the mesh, turbulence model, thermodynamic model and boundary conditions. Subsequently, the CFD approach used to model the jet-ejector behavior is validated using experimental data.

3.1 Working fluid selection

R1234yf has been used as the working fluid in the present study due to its reduced environmental impact (GWP = 4) as well as its widespread use in modern automotive air conditioning systems. It is an energy-efficient replacement for R134a and its implementation requires minor modifications in actual automotive equipment (Lee and Jung, 2012), (Vaghela, 2017). This new generation refrigerant exhibits low toxicity, however, it is flammable so safety measures must be adopted to cope with leaks during service.

3.2 Jet-ejector flow phenomena and geometry description

In the present jet-ejector design, the high-pressure primary flow (7) is expanded in a converging-diverging nozzle reaching sonic conditions at the nozzle throat with a subsequent increase in supersonic level owing to expansion at the diverging section. The subsequent pressure reduction downstream nozzle exit region (8) favors secondary flow entrainment at the suction chamber (2). Only a little fraction of both flows mix in the first instance but the primary flow boundary is clearly delimited creating an apparent converging duct with the wall where secondary flow expands. Once the secondary flow is expanded a mixing process characterized by momentum transference from primary to secondary flow occurs (3). Due to the higher outlet backpressure, additional shockwave pattern appears along the constant area zone. Therefore, the mixed flow returns to subsonic conditions and the static pressure of the mixed flow increases. Mixed flow leaves the ejector with an additional pressure recovery induced by the subsonic diffuser (4).

176 The entrainment ratio, i.e, the ratio between secondary and primary mass flow ($\omega = \dot{m}_s/\dot{m}_p$)
177 has been selected as the reference performance parameter. From the performance perspective,
178 high entrainment ratio values have a positive impact on the cooling capacity and COP. According
179 to Figure 1, cooling capacity and COP of the ejection cycle under investigation are defined as
180 follows:

$$\dot{Q}_{ev} = \dot{m}_s \cdot (h_1 - h_0) \tag{1}$$

181

$$COP = \frac{\dot{Q}_{ev}}{\dot{Q}_{ge} + \dot{W}_{pm}} \approx \frac{\dot{m}_s}{\dot{m}_p} \cdot \frac{(h_1 - h_0)}{(h_7 - h_6)} = \omega \cdot \frac{(h_1 - h_0)}{(h_7 - h_6)} \tag{2}$$

182 It must be noted that the input power to drive the pump has been neglected in the COP
183 definition because it is much lower than the incoming heat power.

184 Figure 3 depicts a schematic view of the axisymmetric jet-ejector prototype under investigation
185 with all the relevant dimensions. The geometric optimization has been carried out for different
186 nozzle exit diameters ($D_{e,3}$), constant mixing diameters ($D_{e,4}$) and nozzle exit positions ($L_{e,2}$)
187 for a fixed nozzle throat diameter ($D_{e,2}$). The primary nozzle throat has remained constant in all
188 simulations, thus fixing the critical mass flow when primary pressure and temperature are
189 maintained.

190

191 The diffuser length and the mixing chamber length have been assigned to ensure negligible
192 gradients of both pressure and Mach number on the radial direction at the jet-ejector outlet.
193 Several preliminary studies concerning the jet-ejector geometry have been conducted to fix
194 some geometric values that do not have a strong influence over the jet-ejector performance. All
195 the dimensions involved in the geometrical design of the jet-ejector are presented in Table 1.

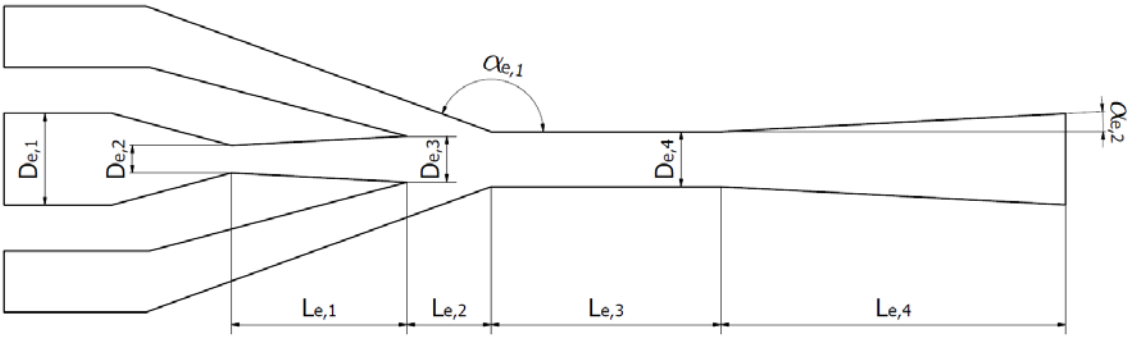

Figure 3. Jet-ejector axisymmetric design

Dimension		Value	Dimension		Value
$\boldsymbol{\alpha_{e,1}}[°]$	Constant	150	$\boldsymbol{D_{e,4}}[\boldsymbol{mm}]$	Variable	[3.2, 3.8]
$\boldsymbol{\alpha_{e,2}}[°]$	Constant	3	$\boldsymbol{L_{e,1}}[\boldsymbol{mm}]$	Constant	11.5
$\boldsymbol{D_{e,1}}[\boldsymbol{mm}]$	Constant	6	$\boldsymbol{L_{e,2}}[\boldsymbol{mm}]$	Variable	[4,7]
$\boldsymbol{D_{e,2}}[\boldsymbol{mm}]$	Constant	1.8	$\boldsymbol{L_{e,3}}[\boldsymbol{mm}]$	Constant	30
$\boldsymbol{D_{e,3}}[\boldsymbol{mm}]$	Variable	[2.6, 3.2]	$\boldsymbol{L_{e,4}}[\boldsymbol{mm}]$	Constant	45

Table 1. Dimensions of the jet-ejector model

The jet-ejector area ratio, that is, the ratio between the mixing chamber area and the primary nozzle throat area, has proven to be one of the most sensitive parameters on ejector performance and its influence over the mixing process has been widely studied in the literature (Varga et al., 2009; Wang et al., 2018). For this reason, it has been treated as a design variable. Additionally, the nozzle exit area determines the expansion level of the primary flow, i.e., Mach number of primary flow leaving the nozzle. The influence over the jet-ejector internal phenomena has proven to be decisive (Ruangtrakoon et al., 2013) so it has been considered as the second geometric variable under investigation. The nozzle exit position (NXP) is also crucial in the jet-ejector operation (Chen et al., 2015) and it must be optimized together with the primary nozzle exit diameter and mixing chamber diameter to maximize the jet-ejector

performance. It must be noted that for a fixed nozzle throat, the mixing chamber diameter ($D_{e,4}$), the primary nozzle exit diameter ($D_{e,3}$) and the nozzle exit position ($L_{e,2}$) govern primary flow expansion as well as the suction and mixing processes of the secondary flow.

A parametric factorial study has been conducted with $D_{e,3}$, $D_{e,4}$ and $L_{e,2}$ to find the best combination in terms of entrainment ratio maximization. The range of these geometric variables is specified in Table 1. The mesh of the computational domain has been adapted for each case according to changes in geometry.

Concerning the weight of the jet-ejector and the hypothetical penalty over the vehicle, Zegenhagen and Ziegler (Zegenhagen and Ziegler, 2015a) reported a gravimetric power density of 0.6-1.3 kW (of cooling capacity)/kg for the jet-ejector considering real equipment. This reference is useful to provide an estimation of the jet-ejector expected mass but it would depend on each particular design. The present jet-ejector is intended to be implemented in a refrigeration system with a cooling capacity of approximately $2kW$. Assuming the aforementioned gravimetric power density, a mass of 1.5 kg could be a reasonable approximation.

3.3 Jet-ejector off-design performance maps

In this subsection, the jet-ejector performance maps representing the entrainment ratio against the operating pressure ratios are introduced. The operating conditions of an ejection cycle intended for ICE intake cooling can change significantly depending on cooling requirements or the ambient conditions. Hence, for this particular application, the ejection cycle operation would be far from being steady and off-design evaluation has a special significance.

Off-design jet-ejector performance is usually evaluated by means of a characteristic surface (Zegenhagen and Ziegler, 2015a, 2015b) which represents the operating pressures expressed as pressure ratios ($\pi_{sp} = P_s/P_p$ and $\pi_{op} = P_o/P_p$) together with entrainment ratio ($\omega = \dot{m}_s/\dot{m}_p$).

241 Resulting operating modes are depicted in Figure 4 keeping constant the primary pressure (P_p)
242 in order to simplify the analysis.
243

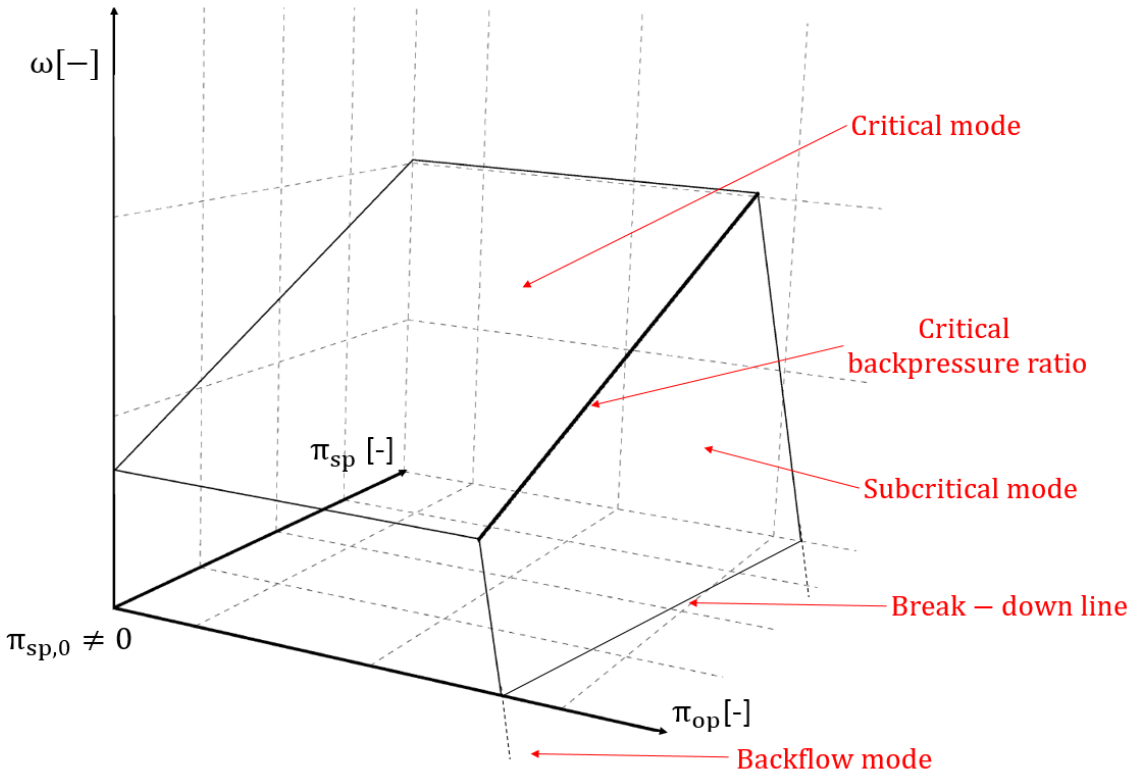

244
245 *Figure 4. Jet-ejector characteristic surfaces*
246

247 According to jet-ejector maps of Figure 4, three different modes can be distinguished: double-
248 choking mode also known as critical mode, single-choking mode, known as subcritical mode and
249 backflow mode. In the double-choking mode, both primary and secondary flows reach
250 supersonic conditions and the entrainment ratio does not depend on the jet-ejector
251 backpressure (outlet pressure) until a certain critical value if the primary pressure is fixed. The
252 primary flow reaches sonic conditions during the expansion on the converging-diverging nozzle
253 and the secondary flow is accelerated to sonic conditions as it passes through a converging duct
254 created by the shockwave structure downstream the primary nozzle. This 'effective area' is

produced at the mixing chamber and its position depends on operating conditions and geometry. Double-choking operating mode corresponds to the desired ejector operating mode.

In single-choking mode, the critical backpressure is exceeded and only the primary flow is choked. In this case, the relatively high backpressure shifts oblique shockwaves induced upstream the diffuser (called second shockwave pattern) toward the primary nozzle, thus affecting the mixing process. Therefore, the entrainment process of the secondary flow is altered and the jet-ejector entrainment ratio is not independent of jet-ejector backpressure. Once the jet-ejector critical backpressure is exceeded secondary mass flow is reduced with the increase of the jet-ejector backpressure. A further increase can lead to the break-down line where no secondary mass flow is entrained. This operating mode should be avoided because slight variations in jet-ejector backpressure can lead to significant performance degradation.

In backflow mode, the break-down pressure (Figure 4) is exceeded and the second shockwave moves upstream affecting primary expanded flow. With the disturbance of primary flow expansion, it tends to penetrate into the secondary duct flowing upstream. It is considered as a malfunctioning mode because the jet-ejector is unable to entrain secondary flow.

When the critical pressure is exceeded the entrainment ratio drops dramatically with the subsequent reduction in cooling capacity and COP. Thus, critical, subcritical and backflow modes are directly dependent on operating conditions and off-design operation can lead to severe performance degradation.

Both critical and subcritical performance maps are expressed in Equations 3-7. The aim of the off-design study is obtaining the fitting coefficients β_{I-VI}. For that purpose, the response of the optimum geometry has been evaluated over different pressure ratios, $\pi_{sp} \in [0.103,0.152]$ and $\pi_{op} \in [0.300,0.376]$.

$$\omega(\pi_{sp}, \pi_{op}) = \frac{\dot{m}_s}{\dot{m}_p} \quad (3)$$

$$\omega_{crit}(\pi_{sp}, \pi_{op}) = \beta_I + \beta_{II} \cdot \pi_{sp} + \beta_{III} \cdot \pi_{op} \quad (4)$$

$$\omega_{scrit}(\pi_{sp}, \pi_{op}) = \beta_{IV} + \beta_V \cdot \pi_{sp} + \beta_{VI} \cdot \pi_{op} \quad (5)$$

$$\omega(\pi_{sp}, \pi_{op}) = \omega_{crit}(\pi_{sp}, \pi_{op}) \quad if \quad \omega_{crit}(\pi_{sp}, \pi_{op}) \leq \omega_{scrit}(\pi_{sp}, \pi_{op}) \quad (6)$$

$$\omega(\pi_{sp}, \pi_{op}) = \omega_{scrit}(\pi_{sp}, \pi_{op}) \quad if \quad \omega_{crit}(\pi_{sp}, \pi_{op}) > \omega_{scrit}(\pi_{sp}, \pi_{op}) \quad (7)$$

3.4 Computational characterization

3.4.1 Numerical simulation setup

Numerical simulations of the jet-ejector internal flow over different geometries and boundary conditions have been accomplished. All the cases under investigation have been simulated using a computational fluid dynamics (CFD) code based on the finite volume method. The governing equations are based on mass, momentum and energy conservation. The three-dimensional geometry of this particular problem has been taken into account by considering a 2D domain with axisymmetry. Steady-state conditions and compressible turbulent flow are assumed since the flow inside the jet-ejector is thought to be supersonic according to the operating pressures. The computational code assumes that the fluid behaves as superheated vapor, supercritical fluid, or liquid. Two-phase subcritical flow conditions, where vapor coexists with liquid, are not supported. In the event of two-phase flow during primary nozzle expansion, the calculation is automatically stopped.

As the working fluid used in the jet-ejector is R1234yf and the operating pressures are relatively high, the perfect gas assumption may not be an accurate approach (Zegenhagen and Ziegler, 2015c). Instead, libraries containing thermodynamic properties of R1234yf are dynamically

loaded into the solver when real gas models are activated. This causes certain difficulties to start and stabilize the calculations. First-order upwind spatial discretization schemes for turbulence and conservation equations are used in the first instance and then switched to a second-order scheme when stability is attained. At the early stages of calculation, the SIMPLE pressure-velocity coupling scheme is considered and then switched to a Coupled scheme after reaching final boundary conditions and stabilization. Least Square Cell-Based is selected as gradient scheme and diffusion terms are discretized following a second-order central difference form. The pressure-based coupling model has been employed because current implementations of this approach have been reformulated in order to work successfully with high Mach number compressible flow. Furthermore, satisfactory results implementing this approach when simulating jet-ejector internal flow have been reported in the literature (Croquer et al., 2016). Density-based formulations have been also tested but offered poor performance in terms of stability.

The Reynolds Averaged Navier Stokes (RANS) approach has been employed in all simulations, and the standard $k-\epsilon$ has been selected as the turbulence model. Despite it is not the most recommended turbulence model while simulating supersonic flow in jet-ejectors it has proved to do an accurate description of phenomena occurring inside the jet-ejector as well as accurate predictions of global flow parameters like entrainment ratio (Besagni et al., 2015; Croquer et al., 2016; Gagan et al., 2014; Hakkaki-Fard et al., 2015). Standard wall functions have been considered as the near-wall formulation scheme in accordance with the turbulence model and y^+ values (Besagni and Inzoli, 2017).

A quadrilateral structured mesh with wall refinement (Figure 5) is selected due to the prevalence of axial flow. Global skewness, orthogonal quality and aspect ratio are checked as quality indicators. The number of cells of the computational domain is around 55,000 in all simulations with slight variations due to the different dimensions of each geometry in the parametric study.

The influence of the number of elements is evaluated by comparing the Mach number along the jet-ejector axis and the entrainment ratio of three cases with different mesh refinement (Figure 6). There are small discrepancies in the position and magnitude of strong shockwaves, however, differences in entrainment ratio are lower than 1% with respect to the case with the highest number of cells.

The discrepancies found in Mach number distribution in some axial positions can be attributed to the strong gradients occurring due to the shockwave pattern. It is common in the literature to carry out a detailed mesh refinement in these particular zones to capture the shockwave structure. In the present paper, priority was given to the computational economy due to the high number of simulations that were required to perform an exhaustive optimization of the jet-ejector internal geometry. These minor differences are considered as admissible so the mesh with the lower number of elements (54,600) is selected according to the following criteria:

- The flow phenomena occurring inside the jet-ejector is described only from a qualitative point of view. Therefore, the main trends described on the flow pattern when the jet-ejector internal geometry is modified would remain valid, regardless of the slight discrepancies in the position and magnitude of strong shockwaves.
- The global performance of the jet-ejector is computed from a quantitative point of view by using the jet-ejector entrainment ratio. The validation process as well as the low discrepancies between the three meshes under consideration (less than <1%) guarantee that this global parameter is correctly predicted.

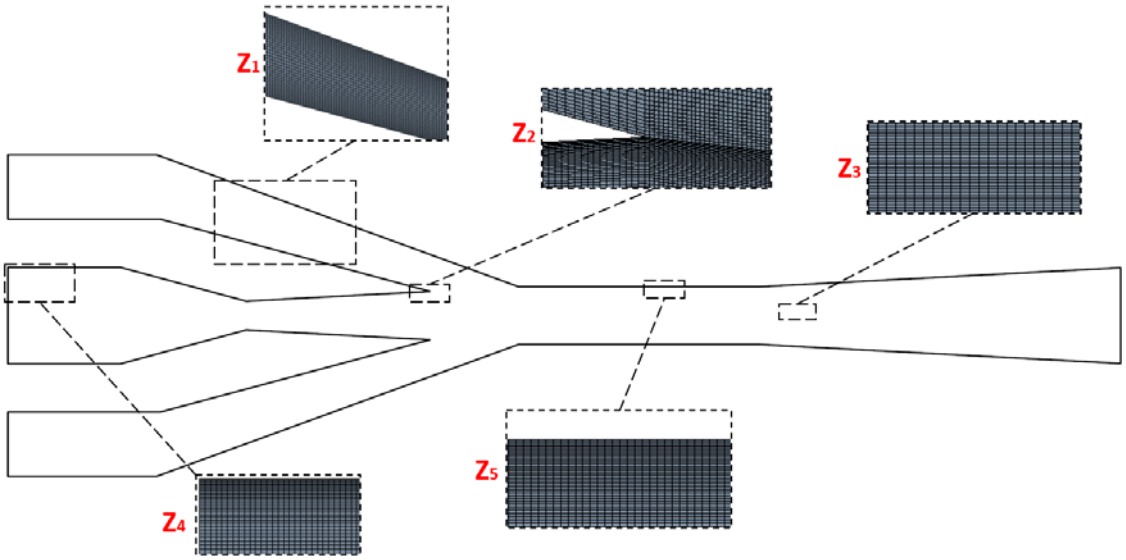

Figure 5. Details of the mesh grid. The element size in the radial direction in each zone corresponds to 1.3e-4 m (Z_1), 5e-5m (Z_2), 4e-5m (Z_3 near the axis), 1e-4 m (Z_4), 2e-5 (Z_5 near the wall).

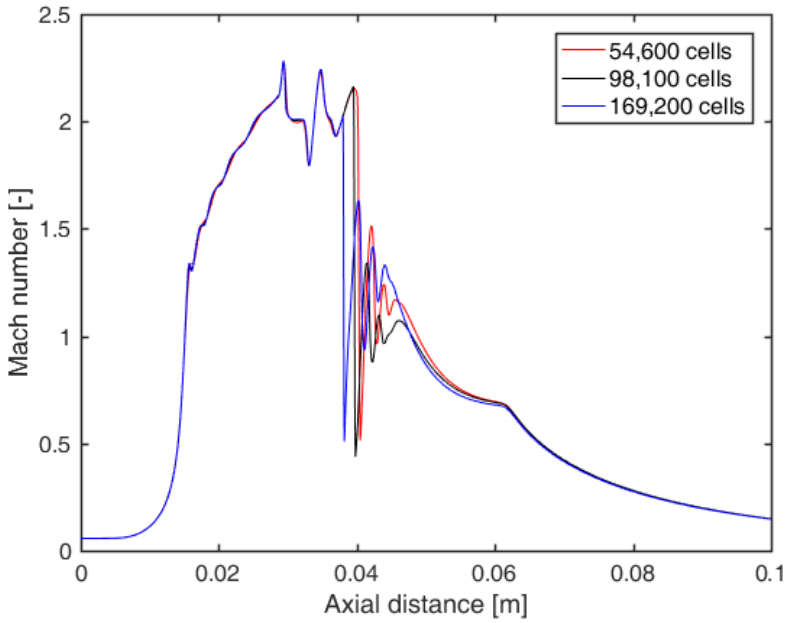

Figure 6. Mach number along the jet-ejector axis for cases with different mesh refinement

3.4.2 Boundary conditions

The jet-ejector operating pressures/temperatures have been selected depending on cooling requirements and ambient conditions. Table 2 summarizes the reference operating conditions (expressed as saturation conditions) considered to perform the computational calculations.

Working Fluid: R1234yf	Value	Units	State number in Figure 1
Condensing pressure (mixed flow)	10.7	[bar]	(4)
Condensing temperature (mixed flow)	42	[$°C$]	(4)
Evaporating pressure (secondary flow)	3.2	[bar]	(1)
Evaporating temperature (secondary flow)	0	[$°C$]	(1)
Generating pressure (primary flow)	30.6	[bar]	(7)
Generating temperature (primary flow)	89.7	[$°C$]	(7)

Table 2. Reference boundary conditions considered in the CFD simulations

The values shown in Table 2 predetermine the maximum achievable performance of the designed jet-ejector and they have been selected according to the following criteria:

- To determine the condensing temperature (42 $°C$) an ambient temperature of 30 $°C$ has been considered as well as a pinch point of approximately 10 $°C$ at the heat exchanger and some degree of liquid subcooling. This is a reasonable outdoor temperature during summer periods in warm climates.
- To determine the evaporating temperature (0 $°C$) a pinch point of 10 $°C$ at the heat exchanger has been assumed. Therefore, the jet-ejector is designed to cool the intake line temperature down to 10 $°C$.
- A priori, there is no constraint to select the generating temperature because the exhaust line shows a high thermal level. A relatively high primary pressure has been chosen in order to reduce the outlet-primary flow pressure ratio ($\pi_{op} = 0.35$) and subsequently to prevent the jet-ejector from operating in subcritical mode. However, this value is not

necessarily the optimum one. It has been fixed just to reduce the number of degrees of freedom involved in the optimization process. If another generating pressure was selected the optimum jet-ejector geometry might differ from the one found in the present paper. Concerning the off-design analysis, the primary pressure could be affected if there was a change in heat power availability in the exhaust line. This event often happens in a standard driving behavior because the ICE operating point is constantly changing. In such a case the maximum primary pressure might be limited and a severe performance degradation might occur if the jet-ejector operates within the subcritical or the backflow modes. Nevertheless, the ICE transient conditions play a major role when assessing the evolution of the exhaust line temperature and this analysis exceeds the aim of the present paper.

Primary and secondary inlets are set to static pressure boundary condition and the outlet zone of the jet-ejector is set to total pressure (see Figure 7). Total and static values in both inlets are supposed to be essentially the same because the inlet velocity is neglected as a common approximation (Croquer et al., 2016). Hence, the mass flow rates passing through the jet-ejector are a result of the three pressure boundary conditions.

Total temperature is also imposed on both inlets and it is equal to static temperature following the previous criteria. A superheating temperature of 10 $°C$ has been assumed in the primary and secondary flows to avoid condensation in the expansion process occurring downstream.

In order to reduce the calculation time and to take into account the 3D geometry domain, the axisymmetric condition is assigned at the jet-ejector mid-line since 3D effects can be neglected (Pianthong et al., 2007).

The walls are defined as adiabatic, impermeable and smooth surfaces in which the no-slip condition is satisfied. A schematic representation of the wall domain is represented in Figure 7.

To sum up, the following boundary conditions are assigned in the CFD cases to solve the governing equations:

- Domain with axisymmetry.
- Two pressure inlet assignments (primary flow and secondary flow). Static pressure and static temperature are imposed in these pressure inlets.
- One pressure outlet assignment (mixed flow).
- Wall to bound fluid and solid regions.

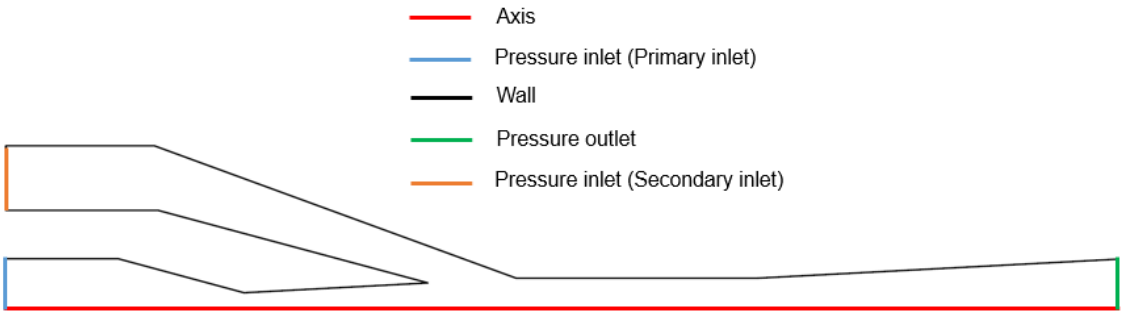

Figure 7. Boundary condition assignment on geometry

3.4.3 Thermodynamic model and convergence criteria

The thermodynamic properties of R1234yf stored at CFD code are based on the formulation of Richter et al. (Richter et al., 2011). A real gas model has been considered instead of an ideal gas assumption since absolute pressure inside the jet-ejector is assumed to be relatively high and in this situation, the behavior of both models might not be similar. The fluid thermodynamic variables can be determined accurately in the temperature range between -53 $°C$ and 137 $°C$ and pressure values up to 300 bar. The properties of the refrigerant are implemented in the CFD code by means of NIST libraries. Due to the NIST real gas model approach, the solution converges at a slower rate than when running an ideal gas flow. The converging process of the calculation is also more unstable. The solution diverges if flow properties exceed the bounded range even though the state is physically valid. In order to avoid an aggressive convergence strategy the

boundary conditions are changed dynamically. Different transitions have been performed in order to progressively achieve the desired pressure boundary conditions in both inlets and the outlet. Gradual pressure increments in the primary inlet are the best strategy especially in the early stages of calculation since the solution oscillates. Five criteria are examined to consider each case as converged:

- Inlet and outlet mass flow rates do not vary with iterations, i.e., values are constant.
- The balance between the inlet and outlet mass flow rates is at least three orders of magnitude lower than the minimum inlet mass flow.
- Calculation residuals are stable.
- Mach number at the converging-diverging nozzle throat is constant.
- The values of prescribed pressure and temperature boundary conditions do not vary with iterations.

Around 20,000 iterations are required in order to satisfy previous conditions but strong dependence with the jet-ejector operating mode has been found. The mass flow rate balance and secondary mass flow rate stabilization are the limiting factors. Those cases in which the jet-ejector operates in critical mode exhibit secondary mass flow stabilization in fewer iterations. However, those cases in which boundary conditions lead to the subcritical operating mode usually require more iterations.

3.4.4 Computational model validation

The previous numerical approach has been validated with two experimental datasets available in the literature (García Del Valle et al., 2014; Hakkaki-Fard et al., 2015). Discrepancies in entrainment ratio have been evaluated between the present CFD approach and the three jet-ejector prototypes presented in the research work of Hakkaki-Fard et al. (Hakkaki-Fard et al., 2015) and the geometry “A” of the results reported by García del Valle et al (García Del Valle et

al., 2014). The relative deviation in the entrainment ratio between the simulated points and the former experimental study does not exceed 7.2%. When the deviations are compared with the latter research work the discrepancies do not exceed 13.2% but the CFD simulations tend to slightly overestimate the jet-ejector entrainment ratio. Regardless of the small discrepancies, these results demonstrate that the CFD setup is providing reliable results.

The geometry and operating pressures of the jet-ejector under investigation in the present study are comparable to those of the research works used for validation. The working fluid used in the present paper (R1234yf) and the refrigerant used to validate the simulations (R134a) show comparable thermodynamic properties. In fact, R1234yf is the environmentally-friendly replacement of R134a in many applications.

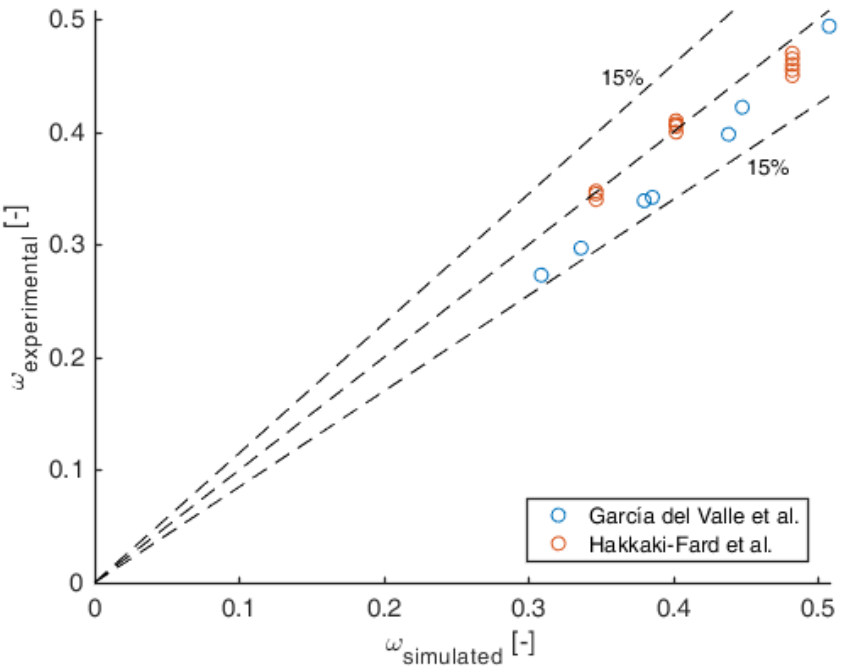

Figure 8. Deviations of the present CFD approach and experimental data from the literature

4. JET-EJECTOR REFRIGERATION SYSTEM MODELING

In this section, the theoretical model used to determine the maximum achievable cooling capacity when the jet-ejector cycle operates against a high ambient temperature is presented.

457 The influence of ambient conditions in the overall cycle performance has been tested by using
458 the 1D thermodynamic model and the optimization procedure investigated by Galindo et al.
459 (Galindo et al., 2019) as well as the non-dimensional jet-ejector maps of the present paper.

460 The refrigeration system aims to reduce the intake air temperature downstream of the
461 intercooler of the ICE from $\sim 40\ ^{\circ}C$ to $\sim 0\ ^{\circ}C$ with a resulting cooling capacity of approximately
462 1.7 kW for the operating point of 2000 rpm and 50% load.

463 The cycle layout corresponds to the scheme depicted in Figure 1. The ambient conditions
464 sensitivity analysis has been carried out for a frequent engine operating point (2000 rpm, 50%
465 load) taking as boundary conditions in the engine side experimental measurements of the
466 temperature and mass flow at the intake and exhaust lines (see Table 3). The engine data come
467 from an experimental campaign carried out on an engine test bench in order to characterize the
468 ICE performance operating under several engine loads and speeds.

469 The inputs required to solve the cycle are shown in Table 4 and are varied dynamically by the
470 algorithm MOGA-II (Multi-Objective Genetic Algorithm) to find those feasible operating points
471 that minimize charge air temperature. The MOGA-II is widely used in engineering applications
472 and other areas as an optimization tool (Poles et al., 2007). The solution constraints, as well as
473 the general solving procedure, are available in the research paper referenced before (Galindo et
474 al., 2019). The aforementioned inputs (thermodynamic variables and degrees of freedom) are
475 shown in Table 4 and correspond to the expansion valve pressure drop (ΔP_v), the liquid pump
476 pressure ratio (k), the fraction of available heat at the exhaust line (κ), the superheating
477 temperature of the evaporator in the ejection cycle side ($T_{sup,1}$) and the jet-ejector scaling
478 factor (λ).

479 An ambient temperature of 30 $^{\circ}C$ has been set as the reference condition, that is, the optimum
480 size of the jet-ejector in all the simulations corresponds to the ejection cycle coupled to the ICE
481 working with the mentioned ambient temperature. Then, the overall cycle performance is

reassessed when the ambient temperature varies from 31°C to 38°C maintaining a fixed jet-ejector size. This off-design modeling approach has been presented in detail by Galindo et al. (Galindo et al., 2019).

Parameter	Description	Value
$\dot{m}_{in}[kg \cdot s^{-1}]$	Engine intake mass flow	0.042
$\dot{m}_{ex}[kg \cdot s^{-1}]$	Engine exhaust mass flow	0.044
$T_{i,in}[°C]$	Evaporator inlet temperature at the engine side	40.5
$T_{i,ex}[°C]$	Generator inlet temperature at the engine side	417

Table 3. Engine data used as boundary conditions. The operating point corresponds to 2000 rpm, 50% load

Parameter	Lower limit	Upper limit
$\Delta P_v[bar]$	7	14
$k[-]$	2.5	4.5
$\kappa[-]$	0	1
$T_{sup,1}[°C]$	0	60
$\lambda[-]$ $(*)$	0.5	2

Table 4. Cycle variables modified by the genetic algorithm MOGA-II. (*) This variable is a degree of freedom only when the reference ambient condition is considered.

5. RESULTS

5.1 Determination of the jet-ejector optimum geometry

Three key dimensions are involved simultaneously in the optimization process as described in Section 3: nozzle exit diameter, $D_{e,3} \in [2.6\ mm, 3.2\ mm]$, mixing chamber diameter, $D_{e,4} \in [3.2\ mm, 3.7\ mm]$, and nozzle exit position, $L_{e,2} \in [4\ mm, 7\ mm]$. The influence of $D_{e,3}$ and $D_{e,4}$ over the entrainment ratio is presented in Figure 9 by means of interpolation of scattered data which passes through the simulated points for the optimum nozzle exit position ($L_{e,2} = 5.5\ mm$). Figure 10 depicts the sensitivity analysis of entrainment ratio with the variation of nozzle exit position ($L_{e,2}$) after finding for each case the optimum combination of nozzle exit diameter ($D_{e,3}$) and mixing chamber diameter ($D_{e,4}$).

The relatively low value of optimum entrainment ratio ($\omega_{max} = 0.139$) in comparison with other studies can be attributed to the low secondary-primary pressure ratio and the relatively high outlet-primary pressure ratio.

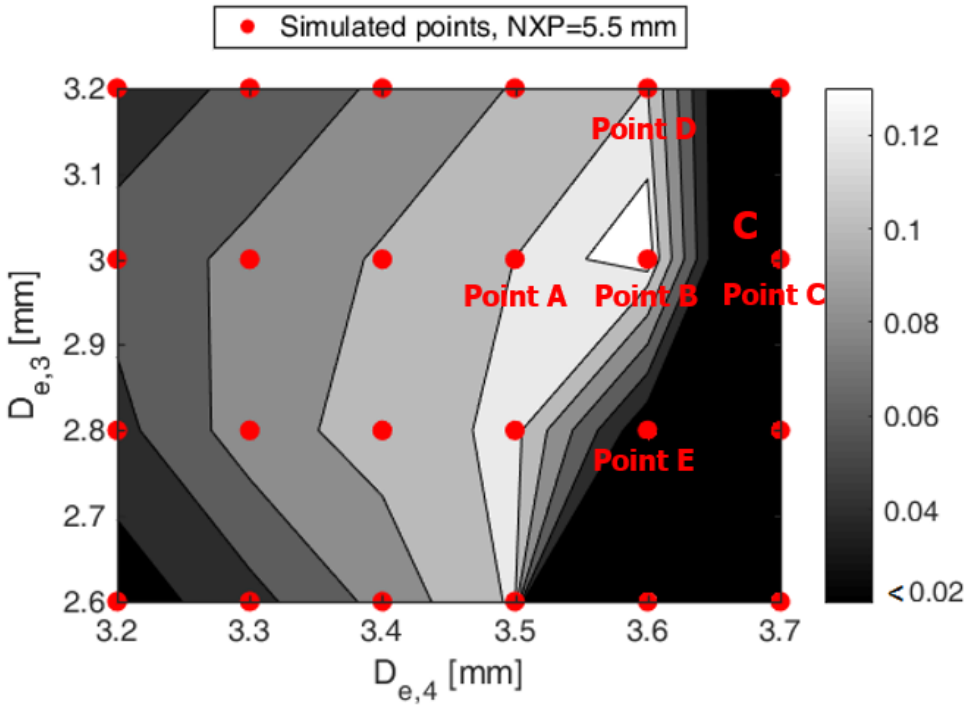

Figure 9. Entrainment ratio contours over nozzle exit diameter and mixing area diameter. A) $D_{e,3} = 3\ mm$, $D_{e,4} = 3.5\ mm$, B) $D_{e,3} = 3\ mm$, $D_{e,4} = 3.6\ mm$, C) $D_{e,3} = 3\ mm$, $D_{e,4} = 3.7\ mm$, D) $D_{e,3} = 3.2\ mm$, $D_{e,4} = 3.6\ mm$, E) $D_{e,3} = 2.8\ mm$, $D_{e,4} = 3.6\ mm$

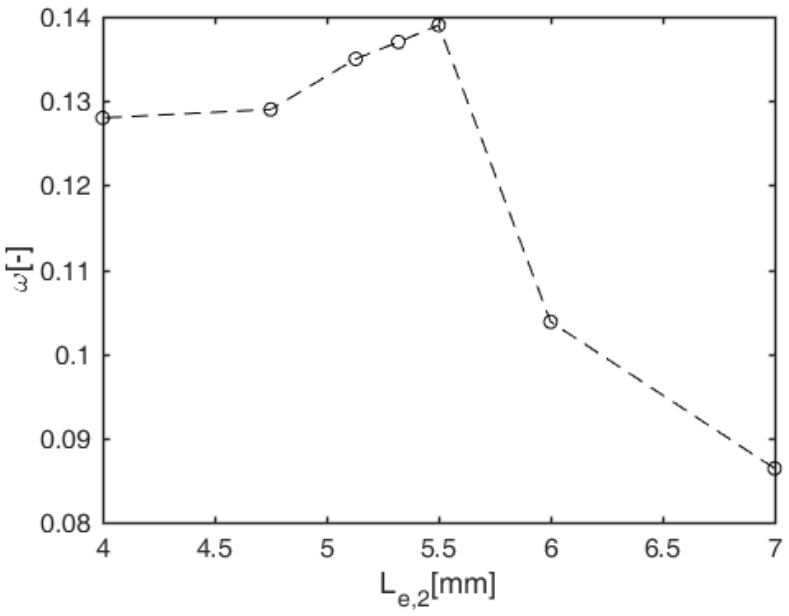

Figure 10. Optimum entrainment ratio for each nozzle exit position ($L_{e,2}$) submitted to study

Flow pattern in non-optimized geometries

Mach contours are depicted in Figure 11 for mixing chamber diameters ($D_{e,4}$) of 3.5 mm, 3.6 mm (case with optimum entrainment ratio) and 3.7 mm with a constant nozzle exit diameter of 3 mm and constant nozzle exit position ($L_{e,2} = 5.5$ mm). These cases correspond with the Points A, B, and C points of Figure 9. The case with a mixing chamber diameter of 3.5 mm (Figure 11) produces an interaction between jet core and the jet-ejector wall, reducing effective area and preventing secondary flow from being entrained. The reduction of entrainment ratio, in this case, has been quantified in 13.3 % with respect to the reference (optimum). On the opposite, the jet-ejector with mixing chamber diameter higher than optimum (3.7 mm), inhibits the entrainment of secondary flow by means of a recirculation bubble placed in a section downstream of the primary nozzle exit plane (see Figure 11). As a result effective area between

the jet-ejector wall and the jet core is also reduced and the secondary flow cannot be entrained (negative values of entrainment ratio are found). Point B (Figure 11) shows the highest entrainment ratio and it corresponds to a trade-off between the flow phenomena exposed before. It demonstrates that for this particular operating conditions and converging-diverging nozzle area ratio an optimum mixing chamber diameter exists.

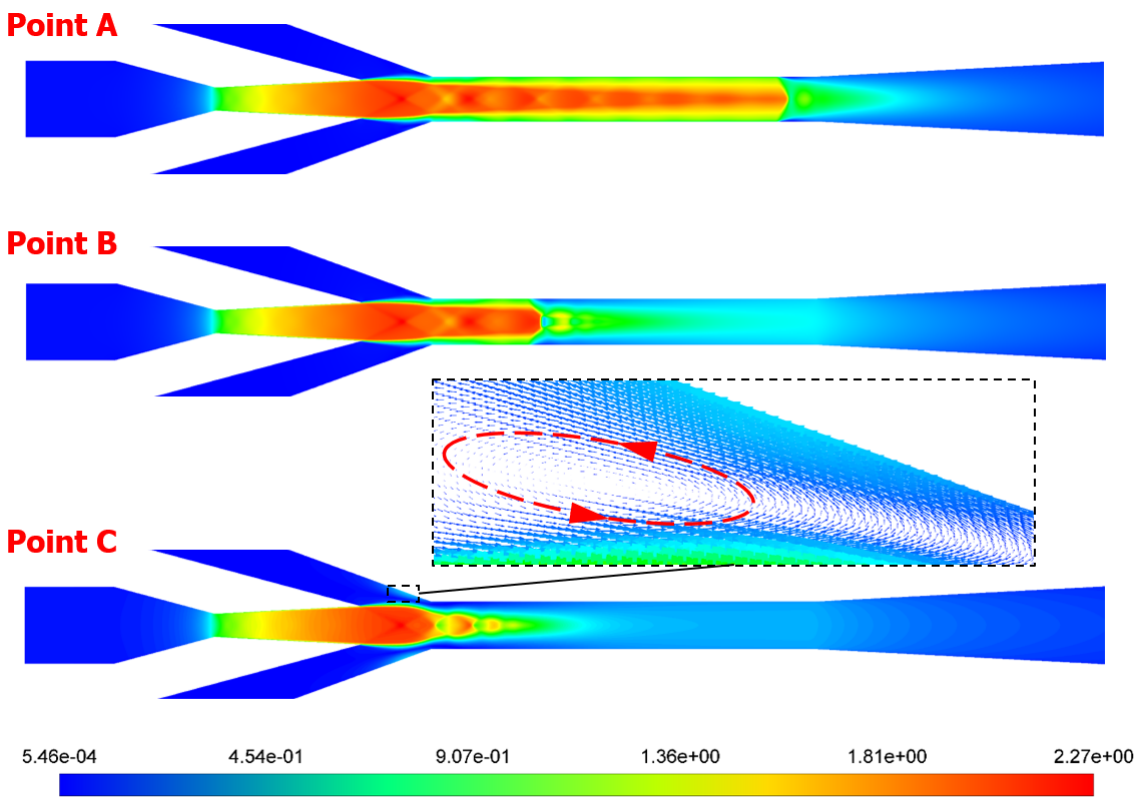

Figure 11. Mach contours over different mixing diameters with $D_{e,3} = 3\ mm$. A) $D_{e,4} = 3.5\ mm$, B) $D_{e,4} = 3.6\ mm$, C) $D_{e,4} = 3.7\ mm$

Figure 12 shows Mach contours for nozzle exit diameter ($D_{e,3}$) of 2.8 mm, 3 mm and 3.2 mm with constant nozzle throat diameter ($D_{e,2}$) of 1.8 mm, fixed mixing diameter ($D_{e,4}$) of 3.6 mm and fixed nozzle exit position ($L_{e,2} = 5.5$ mm). These cases correspond with the Points D, B and E of Figure 9. The first geometry represented in Figure 12 (Point D) shows a divergence in expansion angle which is indicative of under-expanded flow. The divergence angle depends on

541 the pressure difference between the flow leaving nozzle and the flow conditions downstream.
542 As a consequence, additional expansion is produced downstream the exit plane of the nozzle
543 with the subsequent increase of Mach number. Unlike the under-expanded nozzle geometry,
544 the flow pattern of the Point E (Figure 12) reveals that the flow leaves the nozzle with a
545 convergence angle, thus over-expansion occurs. Furthermore, the supersonic level attained at
546 oblique shock pattern downstream the nozzle is not as strong as the case with an under-
547 expanded wave which is a feature of over-expanded waves.

548 Increased momentum at the jet core owing to the higher exit Mach number results in
549 improvement of critical pressure, however, the expansion of jet core affects the secondary flow
550 and produces a partial blockage of the secondary duct limiting the entrainment ratio. The
551 optimum geometry in terms of entrainment ratio corresponds to Point B in Figure 12, that is, an
552 intermediate case between Point D and Point E. In percentage terms, the reduction of
553 entrainment ratio with respect to optimum geometry (B) in cases D and E corresponds to 13.2%
554 and 85.1%, respectively.

555 From the parametric study already mentioned it can be inferred that a great dependence on jet-
556 ejector dimensions exists and precision during the manufacturing process is essential.
557 Manufacturing deviations of only 0.1 mm (<10%) can lead to significant variations in the
558 entrainment ratio.

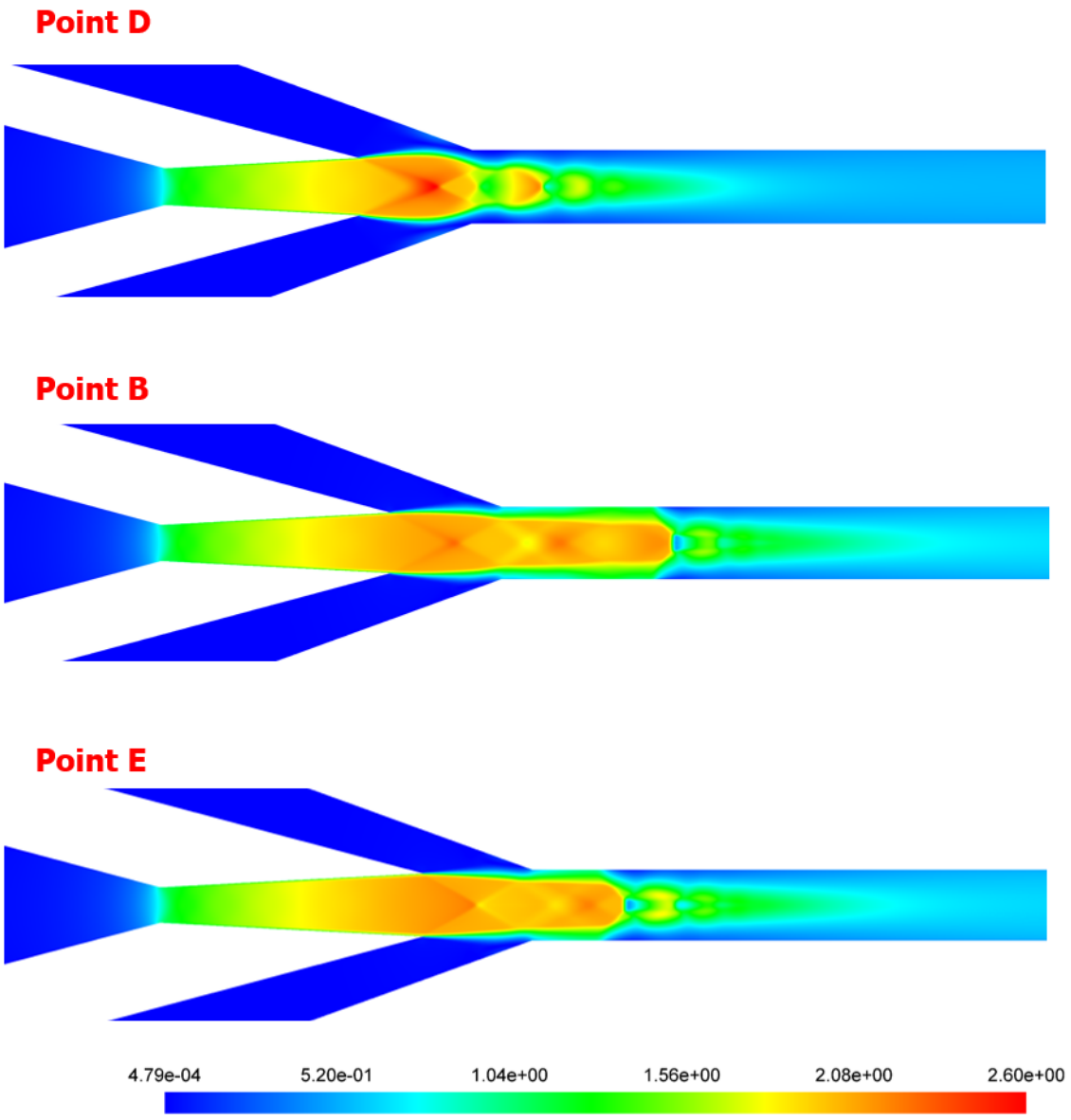

Figure 12. Mach contours over different nozzle exit diameters with $D_{e,4} = 3.6\ mm$. D) $D_{e,3} = 2.8\ mm$, B) $D_{e,3} = 3\ mm$, E) $D_{e,3} = 3.2\ mm$

5.2 Jet-ejector off-design performance

To carry out the off-design performance evaluation, the primary flow pressure (P_p) has been set to 30.6 bar in all the simulations in order to facilitate the analysis of the results. The secondary flow pressure (P_s) has ranged from 3.15 bar to 4.65 bar keeping a constant value for each set of data. Therefore, for a fixed secondary-primary pressure ratio (π_{sp}), the outlet-primary pressure

ratio (π_{op}) has been varied by changing the jet-ejector backpressure. At least three points at critical and subcritical modes have been simulated for each set of data and the results have been represented in Figure 13. Resulting fitting coefficients are presented in Table 5. It should be noted that as π_{sp} increases critical backpressure is expected to appear at higher π_{op} values since mixed flow momentum increases. Because of this, the jet-ejector with $\pi_{op} = 0.36$ operates in critical mode if $\pi_{sp} = 0.152$ but otherwise operates in subcritical mode if $\pi_{sp} = 0.12$.

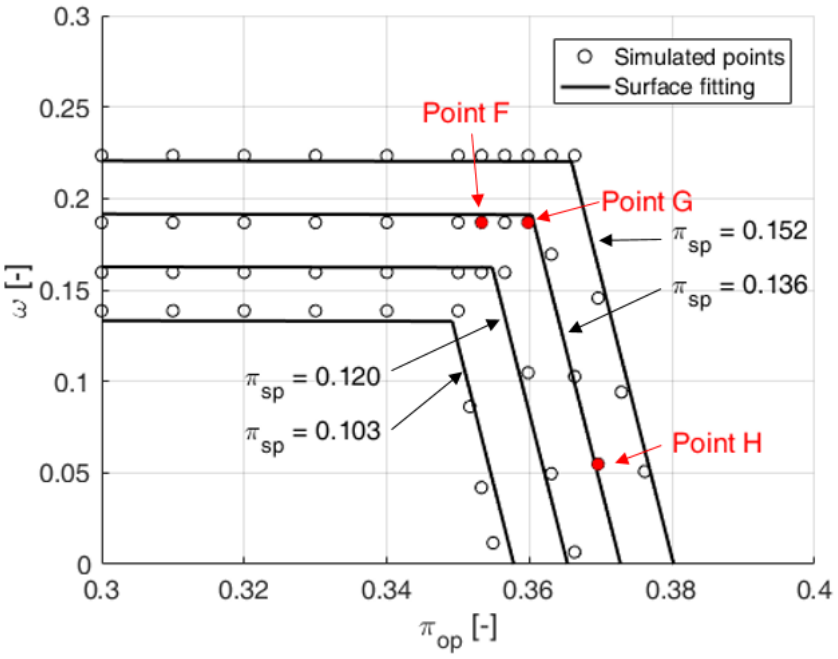

Figure 13. Off-design pressure results with corresponding fitted critical and subcritical surfaces.

$\boldsymbol{\beta_I}$	-0.0476	$\boldsymbol{\beta_{IV}}$	4.771
$\boldsymbol{\beta_{II}}$	1.773	$\boldsymbol{\beta_V}$	6.976
$\boldsymbol{\beta_{III}}$	-0.0063	$\boldsymbol{\beta_{VI}}$	-15.34

Table 5. Fitting coefficients for critical and subcritical characteristic surfaces

The root mean squared error (RSME) has been used as a quality indicator for fitting both critical and subcritical surfaces. Obtained values ($RSME_{crit} = 0.0041, RSME_{scrit} = 0.020$) prove the accuracy of the present approach.

The results of Figure 14 show Mach number contours representing the effect of backpressure keeping constant primary and secondary inlet pressure, with 30.6 bar and 4.15 bar ($\pi_{sp} = 0.136$), respectively. Thus, the flow behavior over characteristic cases is analyzed. It should be noted that two cases represented in Figure 14 (Point F and Point G) are operating in critical mode, i.e, double-choking mode with constant entrainment ratio. As backpressure increases the second series of oblique shocks, that is, shockwave pattern that appears at the constant mixing area region moves upstream without having an influence on the mixing process as can be seen in Figure 14 (Point F and Point G). When the critical backpressure is exceeded and the second series of shockwaves interact with the mixing process, the secondary flow is no longer choked and the secondary mass flow is dramatically reduced (Point H of Figure 14).

Comparing the Points F and G working on critical mode with reference operating pressures ($P_p = 30.6\ bar, P_s = 3.15\ bar, P_o = 10.7\ bar$) an improvement of entrainment ratio of 34.8% is observed which is consistent with critical mode representation since $\pi_{sp} > \pi_{sp,ref}$. In contrast, Point H working on subcritical mode suffers a significant deterioration in the entrainment ratio.

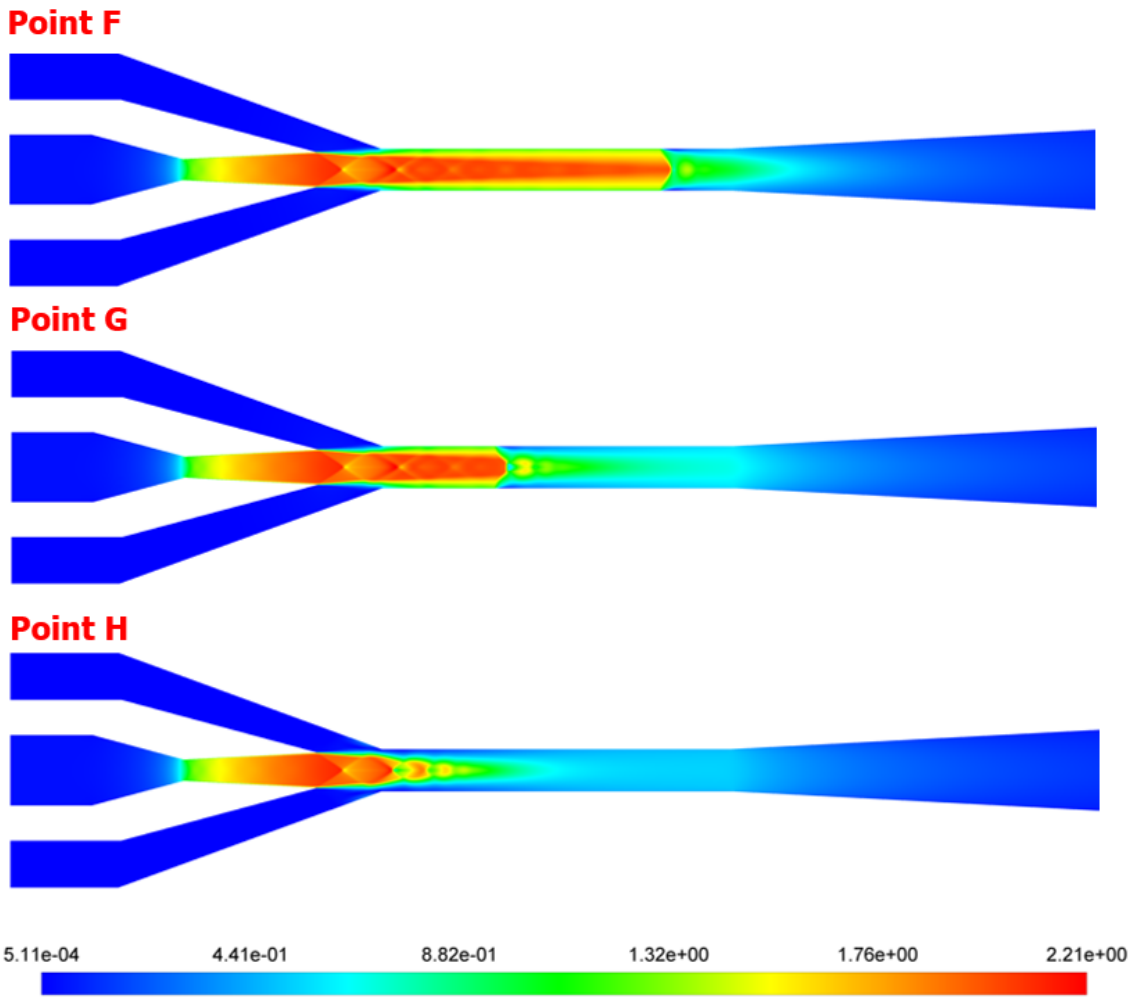

Figure 14. Mach contours over different backpressure with fixed primary flow inlet pressure P_p =30.6 bar, and secondary inlet flow pressure P_s =4.15 bar. G) P_o =10.81 bar, H) P_o =11.01 bar, I) P_o =11.31 bar

5.3 Overall cycle evaluation with off-design ambient temperatures

The minimum achievable charge air temperature in each ambient condition is schematically depicted in Figure 15 and Figure 16. When the ambient temperature ranges between 30°C and 31°C the jet-ejector works in critical operating mode and the desired cooling demand can be attained. Indeed, an engine charge air temperature of 4.6°C ($COP = 0.113$) can be achieved if the ambient temperature is lower than 31°C. On the contrary, when an ambient temperature of 31°C is exceeded a significant performance degradation is observed since the jet-ejector works in subcritical mode. In this situation, the critical backpressure is exceeded and the jet-

ejector entrainment ratio decreases steeply (see Figure 15 and Figure 16). In this case, the minimum achievable temperatures range between 6.3°C and 26.3°C. When the ambient temperature (and therefore the condensing pressure) is increased it is observed that the genetic algorithm tends to increase secondary flow evaporating pressure in order to improve the entrainment ratio by avoiding the break-down line of the jet-ejector subcritical map.

In view of the above, a high dependence with ambient temperature exists and the jet-ejector must be designed carefully to prevent the ejection cycle from operating in the subcritical mode. Otherwise, the cooling load can drop dramatically.

It is complicated to carry out a reliable comparison between the present paper and existing research works in the literature because the real improvement potential of the jet-ejector itself and the jet-ejector refrigeration system strongly depends on the design operating conditions and the working fluid. Furthermore, the research papers relative to application of the recovered ICE waste heat to drive a jet-ejector refrigeration system are scarce. Galindo et al. (Galindo et al., 2019) and Zegenhagen and Ziegler (Zegenhagen and Ziegler, 2015a) studied the feasibility of a jet-ejector refrigeration system coupled to an ICE using R134a as working fluid with a numerical approach in a Diesel engine and an experimental approach in a gasoline engine, respectively.

Despite the relatively low COP values reported (maximum of 0.113 in the present paper, maximum of 0.151 in the first research work (Galindo et al., 2019) and 0.26 in the second one (Zegenhagen and Ziegler, 2015a), these studies demonstrate the feasibility of cooling the ICE intake line down to a temperature close to 0°C by using a jet-ejector refrigeration cycle because the exhaust waste heat is abundant in comparison with the required cooling capacity. This paper provides a supplementary point of view: A quantification of the performance degradation that occurs with an optimized jet-ejector design when the outdoor temperature increases.

635

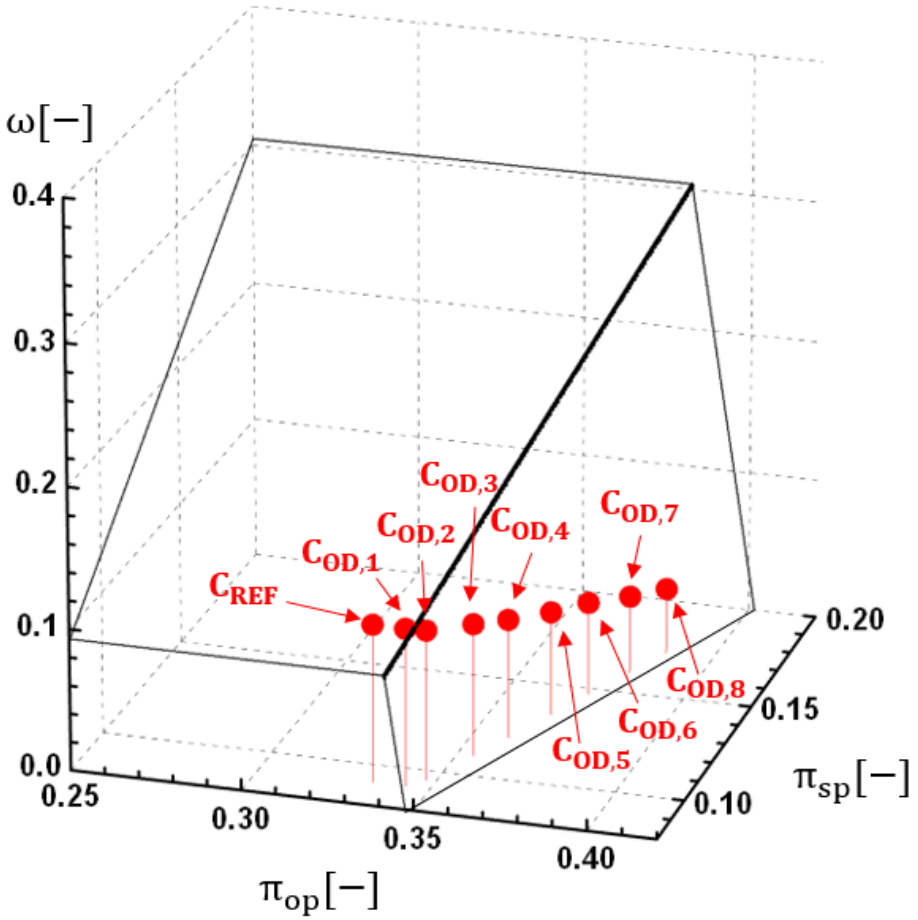

$C_{REF} \rightarrow T_{amb} = 30°C; T_{o,in} = 4.6°C$

$C_{OD,1} \rightarrow T_{amb} = 31°C; T_{o,in} = 4.6°C$

$C_{OD,2} \rightarrow T_{amb} = 32°C; T_{o,in} = 6.3°C$

$C_{OD,3} \rightarrow T_{amb} = 33°C; T_{o,in} = 10.6°C$

$C_{OD,4} \rightarrow T_{amb} = 34°C; T_{o,in} = 13.8°C$

$C_{OD,5} \rightarrow T_{amb} = 35°C; T_{o,in} = 17.4°C$

$C_{OD,6} \rightarrow T_{amb} = 36°C; T_{o,in} = 20.5°C$

$C_{OD,7} \rightarrow T_{amb} = 37°C; T_{o,in} = 23.6°C$

$C_{OD,8} \rightarrow T_{amb} = 38°C; T_{o,in} = 26.3°C$

636

637 *Figure 15. Ejection cycle operating points with different ambient temperature represented over the jet-ejector maps*

638

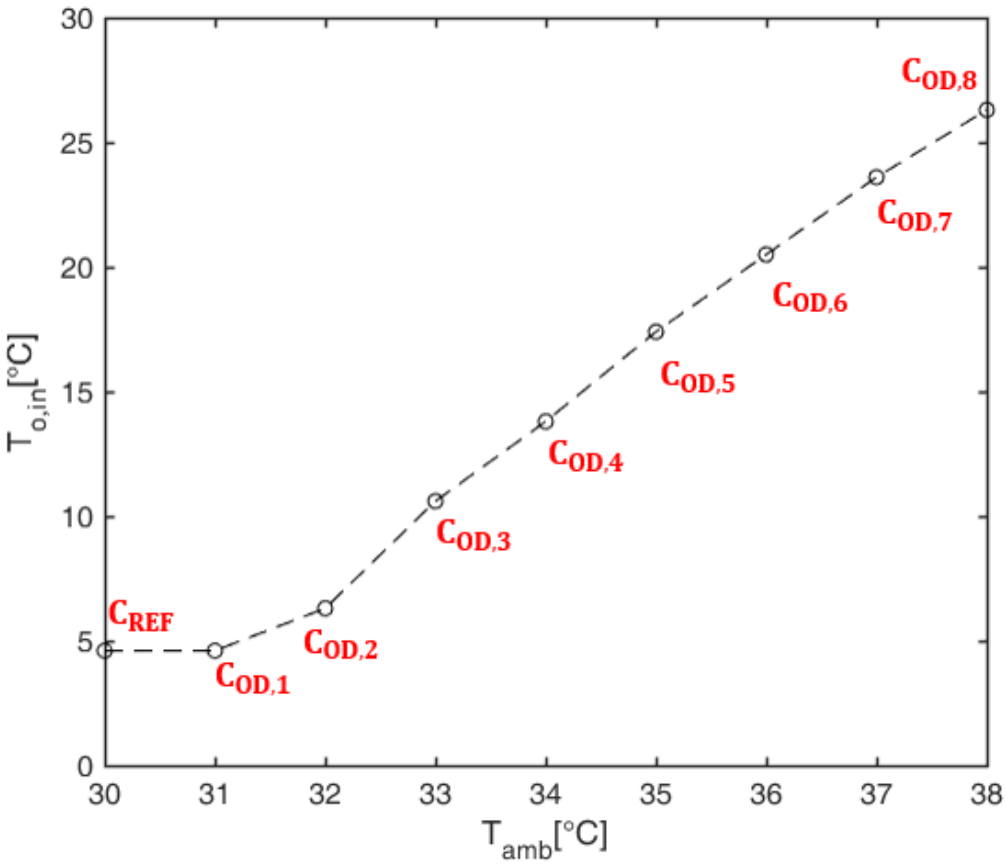

Figure 16. The cooling effect of the ejection cycle over different ambient temperatures

6. CONCLUSIONS

In the present paper, a jet-ejector prototype intended for cooling down an ICE intake for an automotive application has been designed and characterized. In the first instance, a geometric optimization has been performed under specific operating conditions of a passenger vehicle ICE, in terms of thermal power availability and cooling requirements. Subsequently, the optimum geometry has been submitted to off-design operating pressures to obtain the critical and subcritical characteristic surfaces. To conclude, the performance of the overall system has been evaluated against off-design ambient temperatures using the previous jet-ejector design. The main conclusions are outlined below:

- An optimum entrainment ratio of $\omega_{max} = 0.139$ has been obtained for a nozzle exit diameter ($D_{e,3}$), mixing chamber diameter ($D_{e,4}$) and nozzle exit position ($L_{e,2}$) values of

3 mm, 3.6 mm and 5.5 mm, respectively. The relatively low entrainment ratio values can be attributed to the adverse operating pressures. In the non-optimized geometries, the mixing chamber diameter ($D_{e,4}$) is a key factor affecting jet core and wall interaction and consequently entrainment process. Likewise, the nozzle exit diameter ($D_{e,3}$) determines primary flow expansion level and flow structure downstream the nozzle. Hence, the optimum values of previous dimensions are strongly influenced by operating pressures so boundary conditions coming from the ejection cycle must be accurately predicted to maximize performance. Furthermore, the short total length of the jet-ejector (<110 mm) would facilitate a compact-sized system easier to package in a vehicle.

- Simple expressions of both critical and subcritical modes have been demonstrated to be a feasible approach to model the jet-ejector behavior in off-design operating conditions. This non-dimensional two planar model contains information about the jet-ejector geometry as well as performance and they would remain valid if the jet-ejector scale is modified.
- When the ability of the overall ejection refrigeration system to cool down the intake of an ICE operating at 2000 rpm and 50% load is assessed, it is observed that temperatures near zero Celsius degrees (4.6°C) can be attained at the reference ambient temperature (30°C). However, if the ambient temperature exceeds 31°C then the jet-ejector operates in subcritical mode and the system performance drops dramatically. Despite this, if the system operates with 38°C of ambient temperature it is still possible to generate some cooling capacity. In such a case 26.3°C can be attained at the engine intake line.

Acknowledgements

Authors want to acknowledge to the institution “Conselleria d´Educació, Investigació, Cultura i Esport de la Generalitat Valenciana” and its grant program “Subvenciones para la contratación de personal investigador de carácter predoctoral” for doctoral studies (ACIF/2018/124).

7. BIBLIOGRAPHY

Aghaali, H., Ångström, H.E., 2015. A review of turbocompounding as a waste heat recovery system for internal combustion engines. Renew. Sustain. Energy Rev. 49, 813–824. https://doi.org/10.1016/j.rser.2015.04.144

Aly, S.E., 1988. Diesel engine waste-heat power cycle. Appl. Energy 29, 179–189. https://doi.org/10.1016/0306-2619(88)90027-X

Armstead, J.R., Miers, S.A., 2013. Review of Waste Heat Recovery Mechanisms for Internal Combustion Engines. J. Therm. Sci. Eng. Appl. 6. https://doi.org/10.1115/1.4024882

Bartosiewicz, Y., Aidoun, Z., Desevaux, P., Mercadier, Y., 2005. Numerical and experimental investigations on supersonic ejectors. Int. J. Heat Fluid Flow 26, 56–70. https://doi.org/10.1016/j.ijheatfluidflow.2004.07.003

Besagni, G., Inzoli, F., 2017. Computational fluid-dynamics modeling of supersonic ejectors: Screening of turbulence modeling approaches. Appl. Therm. Eng. 117, 122–144. https://doi.org/10.1016/j.applthermaleng.2017.02.011

Besagni, G., Mereu, R., Chiesa, P., Inzoli, F., 2015. An Integrated Lumped Parameter-CFD approach for off-design ejector performance evaluation. Energy Convers. Manag. 105, 697–715. https://doi.org/10.1016/j.enconman.2015.08.029

Chen, S., Chen, G., Fang, L., 2015. An experimental study and 1-D analysis of an ejector with a movable primary nozzle that operates with R236fa. Int. J. Refrig. 60, 19–25. https://doi.org/10.1016/j.ijrefrig.2015.08.011

Chen, X., Worall, M., Omer, S., Su, Y., Riffat, S., 2013. Theoretical studies of a hybrid ejector CO2compression cooling system for vehicles and preliminary experimental investigations of an ejector cycle. Appl. Energy 102, 931–942. https://doi.org/10.1016/j.apenergy.2012.09.032

Croquer, S., Poncet, S., Aidoun, Z., 2016. Turbulence modeling of a single-phase R134a supersonic ejector. Part 1: Numerical benchmark. Int. J. Refrig. 61, 140–152. https://doi.org/10.1016/j.ijrefrig.2015.07.030

Dolz, V., Novella, R., García, A., Sánchez, J., 2012. HD Diesel engine equipped with a bottoming Rankine cycle as a waste heat recovery system. Part 1: Study and analysis of the waste heat energy. Appl. Therm. Eng. 36, 269–278. https://doi.org/10.1016/j.applthermaleng.2011.10.025

Dong, J., Kang, C.L., Wang, H.M., Ma, H.B., 2016. Experimental Investigation of Steam Ejector System With an Extra Low Generating Temperature. J. Therm. Sci. Eng. Appl. 8. https://doi.org/10.1115/1.4032483

Gagan, J., Smierciew, K., Butrymowicz, D., Karwacki, J., 2014. Comparative study of turbulence models in application to gas ejectors. Int. J. Therm. Sci. 78, 9–15.

https://doi.org/10.1016/j.ijthermalsci.2013.11.009

Galindo, J., Dolz, V., Tiseira, A., Ponce-Mora, A., 2019. Thermodynamic Analysis and Optimization of a Jet Ejector Refrigeration Cycle Used To Cool Down the Intake Air in an Ic Engine. Int. J. Refrig. 103, 253–263. https://doi.org/10.1016/j.ijrefrig.2019.04.019

Galindo, J., Ruiz, S., Dolz, V., Royo-Pascual, L., Haller, R., Nicolas, B., Glavatskaya, Y., 2015. Experimental and thermodynamic analysis of a bottoming Organic Rankine Cycle (ORC) of gasoline engine using swash-plate expander. Energy Convers. Manag. 103, 519–532. https://doi.org/10.1016/j.enconman.2015.06.085

Galindo, J, Serrano, J., Dolz, V., Kleut, P., 2015. Brayton cycle for internal combustion engine exhaust gas waste heat recovery. Adv. Mech. Eng. 7, 168781401559031. https://doi.org/10.1177/1687814015590314

García Del Valle, J., Saíz Jabardo, J.M., Castro Ruiz, F., San José Alonso, J.F., 2014. An experimental investigation of a R-134a ejector refrigeration system. Int. J. Refrig. 46, 105–113. https://doi.org/10.1016/j.ijrefrig.2014.05.028

Glover, S., Douglas, R., Glover, L., McCullough, G., 2014. Preliminary analysis of organic Rankine cycles to improve vehicle efficiency. Proc. Inst. Mech. Eng. Part D J. Automob. Eng. 228, 1142–1153. https://doi.org/10.1177/0954407014528904

Hakkaki-Fard, A., Aidoun, Z., Ouzzane, M., 2015. A computational methodology for ejector design and performance maximisation. Energy Convers. Manag. 105, 1291–1302. https://doi.org/10.1016/j.enconman.2015.08.070

He, S., Li, Y., Wang, R.Z., 2009. Progress of mathematical modeling on ejectors. Renew. Sustain. Energy Rev. 13, 1760–1780. https://doi.org/10.1016/j.rser.2008.09.032

Hsiao, Y.Y., Chang, W.C., Chen, S.L., 2010. A mathematic model of thermoelectric module with applications on waste heat recovery from automobile engine. Energy 35, 1447–1454. https://doi.org/10.1016/j.energy.2009.11.030

In, B.D., Lee, K.H., 2016. A study of a thermoelectric generator applied to a diesel engine. Proc. Inst. Mech. Eng. Part D J. Automob. Eng. 230, 133–143. https://doi.org/10.1177/0954407015576440

Jia, Y., Wenjian, C., 2012. Area ratio effects to the performance of air-cooled ejector refrigeration cycle with R134a refrigerant. Energy Convers. Manag. 53, 240–246. https://doi.org/10.1016/j.enconman.2011.09.002

Lee, Y., Jung, D., 2012. A brief performance comparison of R1234yf and R134a in a bench tester for automobile applications. Appl. Therm. Eng. 35, 240–242. https://doi.org/10.1016/j.applthermaleng.2011.09.004

Luján, J.M., Climent, H., Dolz, V., Moratal, A., Borges-Alejo, J., Soukeur, Z., 2016. Potential of exhaust heat recovery for intake charge heating in a diesel engine transient operation at cold conditions. Appl. Therm. Eng. 105, 501–508. https://doi.org/10.1016/j.applthermaleng.2016.03.028

Mazzelli, F., Little, A.B., Garimella, S., Bartosiewicz, Y., 2015. Computational and experimental analysis of supersonic air ejector: Turbulence modeling and assessment of 3D effects. Int. J. Heat Fluid Flow 56, 305–316. https://doi.org/10.1016/j.ijheatfluidflow.2015.08.003

Mazzelli, F., Milazzo, A., 2015. Performance analysis of a supersonic ejector cycle working with R245fa. Int. J. Refrig. 49, 79–92. https://doi.org/10.1016/j.ijrefrig.2014.09.020

759 Novella, R., Dolz, V., Martín, J., Royo-Pascual, L., 2017. Thermodynamic analysis of an
760 absorption refrigeration system used to cool down the intake air in an Internal
761 Combustion Engine. Appl. Therm. Eng. 111, 257–270.
762 https://doi.org/10.1016/j.applthermaleng.2016.09.084

763 Pianthong, K., Seehanam, W., Behnia, M., Sriveerakul, T., Aphornratana, S., 2007. Investigation
764 and improvement of ejector refrigeration system using computational fluid dynamics
765 technique. Energy Convers. Manag. 48, 2556–2564.
766 https://doi.org/10.1016/j.enconman.2007.03.021

767 Poles, S., Geremia, P., Campos, F., Weston, S., Islam, M., 2007. MOGA-II for an Automotive
768 Cooling Duct Optimization on Distributed Resources, in: Obayashi, S., Deb, K., Poloni, C.,
769 Hiroyasu, T., Murata, T. (Eds.), Evolutionary Multi-Criterion Optimization. Springer Berlin
770 Heidelberg, Berlin, Heidelberg, pp. 633–644.

771 Richter, M., McLinden, M.O., Lemmon, E.W., 2011. Thermodynamic properties of 2,3,3,3-
772 tetrafluoroprop-1-ene (R1234yf): Vapor pressure and p - ϕ - T Measurements and an
773 Equation of State. J. Chem. Eng. Data 56, 3254–3264. https://doi.org/10.1021/je200369m

774 Ruangtrakoon, N., Thongtip, T., Aphornratana, S., Sriveerakul, T., 2013. CFD simulation on the
775 effect of primary nozzle geometries for a steam ejector in refrigeration cycle. Int. J.
776 Therm. Sci. 63, 133–145. https://doi.org/10.1016/j.ijthermalsci.2012.07.009

777 Sargolzaei, J., Pirzadi Jahromi, M.R., Saljoughi, E., 2010. Triple-Choking Model for Ejector. J.
778 Therm. Sci. Eng. Appl. 2. https://doi.org/10.1115/1.4002752

779 Soroureddin, A., Mehr, A.S., Mahmoudi, S.M.S., Yari, M., 2013. An experimental and
780 theoretical study of a jet-pump refrigeration system designed using a new two-
781 dimensional model for the entrainment region of the ejector. Proc. Inst. Mech. Eng. Part
782 A J. Power Energy 227, 486–497. https://doi.org/10.1177/0957650913477092

783 Sriveerakul, T., Aphornratana, S., Chunnanond, K., 2007. Performance prediction of steam
784 ejector using computational fluid dynamics: Part 2. Flow structure of a steam ejector
785 influenced by operating pressures and geometries. Int. J. Therm. Sci. 46, 823–833.
786 https://doi.org/10.1016/j.ijthermalsci.2006.10.012

787 Vaghela, J.K., 2017. Comparative Evaluation of an Automobile Air - Conditioning System Using
788 R134a and Its Alternative Refrigerants. Energy Procedia 109, 153–160.
789 https://doi.org/10.1016/j.egypro.2017.03.083

790 Varga, S., Oliveira, A.C., Diaconu, B., 2009. Influence of geometrical factors on steam ejector
791 performance - A numerical assessment. Int. J. Refrig. 32, 1694–1701.
792 https://doi.org/10.1016/j.ijrefrig.2009.05.009

793 Wang, L., Liu, J., Zou, T., Du, J., Jia, F., 2018. Auto-tuning ejector for refrigeration system.
794 Energy 161, 536–543. https://doi.org/10.1016/j.energy.2018.07.110

795 Wang, L., Yan, J., Wang, C., Li, X., 2017. Étude Numérique Sur L'Optimisation Des Géométries
796 De La Tuyère Primaire D'Un Éjecteur. Int. J. Refrig. 76, 219–229.
797 https://doi.org/10.1016/j.ijrefrig.2017.02.010

798 Yan, J., Cai, W., Li, Y., 2012. Geometry parameters effect for air-cooled ejector cooling systems
799 with R134a refrigerant. Renew. Energy 46, 155–163.
800 https://doi.org/10.1016/j.renene.2012.03.031

801 Zegenhagen, M.T., Ziegler, F., 2015a. Feasibility analysis of an exhaust gas waste heat driven
802 jet-ejector cooling system for charge air cooling of turbocharged gasoline engines. Appl.

803 Energy 160, 221–230. https://doi.org/10.1016/j.apenergy.2015.09.057

804 Zegenhagen, M.T., Ziegler, F., 2015b. Experimental investigation of the characteristics of a jet-
805 ejector and a jet-ejector cooling system operating with R134a as a refrigerant. Int. J.
806 Refrig. 56, 173–185. https://doi.org/10.1016/j.ijrefrig.2015.01.001

807 Zegenhagen, M.T., Ziegler, F., 2015c. A one-dimensional model of a jet-ejector in critical
808 double choking operation with R134a as a refrigerant including real gas effects. Int. J.
809 Refrig. 55, 72–84. https://doi.org/10.1016/j.ijrefrig.2015.03.013

810 Zhu, Y., Cai, W., Wen, C., Li, Y., 2009. Numerical investigation of geometry parameters for
811 design of high performance ejectors. Appl. Therm. Eng. 29, 898–905.
812 https://doi.org/10.1016/j.applthermaleng.2008.04.025

813 Zhu, Y., Jiang, P., 2014a. Experimental and analytical studies on the shock wave length in
814 convergent and convergent-divergent nozzle ejectors. Energy Convers. Manag. 88, 907–
815 914. https://doi.org/10.1016/j.enconman.2014.09.023

816 Zhu, Y., Jiang, P., 2014b. Experimental and numerical investigation of the effect of shock wave
817 characteristics on the ejector performance. Int. J. Refrig. 40, 31–42.
818 https://doi.org/10.1016/j.ijrefrig.2013.11.008

819